Organic Electronics 59 (2018) 288–292

Contents lists available at ScienceDirect

Organic Electronics

journal homepage: www.elsevier.com/locate/orgel

Letter

Combinatorial optimization of evaporated bilayer small molecule organic solar cells through orthogonal thickness gradients

Xabier Rodríguez-Martínez[a], Antonio Sánchez-Díaz[a], Guilin Liu[b,c,**], M.A. Niño[b], Juan Cabanillas-Gonzalez[b], Mariano Campoy-Quiles[a,*]

[a] Institute of Materials Science of Barcelona (ICMAB-CSIC), UAB Campus, Bellaterra, 08193, Spain
[b] Instituto Madrileño de Estudios Avanzados en Nanociencia (IMDEA-Nanociencia), Cantoblanco, Madrid, 28049, Spain
[c] Schoolof Science, Jiangnan University, Wuxi, Jiangsu 214122, China

ARTICLE INFO

Keywords:
Organic photovoltaics
Photocurrent mapping
Raman imaging
Combinatorial screening
Gradient
High throughput evaluation

ABSTRACT

We report on a combinatorial optimization procedure applied to heterojunction small molecule organic solar cells made of evaporated copper phthalocyanine (CuPc) and 3,4,9,10-perylenetetracarboxylic bisbenzimidazole (PTCBI). Our strategy consists of depositing both light harvesting compounds as orthogonally arranged wedge-shaped layers to then determine the optimum thicknesses which yield the highest photoconversion efficiency. The device performance is locally assessed by means of light-beam induced current images. A quantitative model of co-locally measured Raman images allows determining the corresponding local thicknesses of the active layers. The spatial correlation of both datasets (i.e. local photocurrent density and active layer film thicknesses) enables the rapid optimization of the photovoltaic system studied employing a single functional device, reducing in approximately 20 times the use of resources and time.

1. Introduction

Small molecule organic photovoltaics (OPV) are currently investigated as potential candidates for low-cost energy harvesting applications in large-area, flexible substrates. Copper phthalocyanine (CuPc) and 3,4,9,10-perylenetetracarboxylic bisbenzimidazole (PTCBI) constitute one of the most prominent p-type donor and n-type acceptor pair in the field, initially leading to a power conversion efficiency (PCE) of 0.95% [1]. This combination has since become a reference system for evaporated OPV. Most device architectures found in the literature including normal and inverted devices, consist of a multi-layered stack of thermally evaporated films with an embedded bilayer heterojunction of both small molecule semiconductors. Since these layers are evaporated successively, their final thickness determines the PCE of the device depending on the exciton diffusion length and extinction coefficient of each material. Thus, the optimization of this type of bilayer devices represents a paradigmatic example of multi-parametric problem, whose solution has so far been handled by systematic tests involving the fabrication of tens of devices in which some of the parameters are varied individually or simultaneously until finding the maximum device performance [2–5]. Despite the aid of photophysical models to facilitate optimization, the process remains experimentally tedious and time-consuming so as to optimize a single photovoltaic system, not even mentioning its extrapolation to new materials that can potentially result in higher PCE. In addition, new materials are usually synthesized in small quantities constituting an extra bottleneck in the optimization process which demands an efficient use of the available resources.

In this work we follow a combinatorial approach to solve such problem with a single device and find the same optimum thicknesses as those reported elsewhere while employing significantly less time and resources. In order to achieve this, we prepare a bilayer donor-acceptor OPV in which both donor and acceptor layers are evaporated as wedges with thickness gradients varying continuously from 0 to 20 nm and arranging their thickness gradient axis orthogonally [6,7]. We then quantify the thickness of each layer at each point by means of Raman scattering directly in the functional device [8]. Finally, we measure the photocurrent as a function of position with a home-made light beam induced current (LBIC) setup, which enables the spatial correlation of CuPc and PTCBI layer thicknesses with photocurrent (proportional to the PCE) after proper matching of both datasets.

The use of wedge-shaped layers in the optimization of optoelectronic devices has already been applied to lasers [9], OLEDs [10] and solution processed photovoltaics [11]. These examples have demonstrated that the use of gradients is a very promising tool for

* Corresponding author.
** Corresponding author.
E-mail addresses: guilin.liu@imdea.org (G. Liu), mcampoy@icmab.es (M. Campoy-Quiles).

https://doi.org/10.1016/j.orgel.2018.05.007
Received 23 October 2017; Received in revised form 28 March 2018; Accepted 3 May 2018
Available online 16 May 2018

optimization and functionality. We extend the previous work beyond the one-dimensional screening of the active layer thickness to two-dimensional fabrication coupled to imaging of the local geometry and performance. The sweet spot in performance in bilayer structures is mainly determined by the donor and acceptor film thicknesses which corresponds to a trade-off between light absorption, exciton diffusion and charge generation in the functional devices. The here presented two-dimensional evaluation of evaporated bilayer small molecule organic solar cells constitutes an important advance in terms of evaluation time and material requirements.

2. Results and discussion

The studied device architecture consists of a transparent glass substrate with a 30 nm-thick, sputtered indium tin oxide (ITO) layer and a 20 nm layer of poly(3,4-ethylenedioxythiophene):polystyrene sulfonic acid (PEDOT:PSS) spin-coated on top. In order to have a well-controlled layer growth and high quality clean interfaces, organic layers were evaporated in an ultra-high vacuum (UHV) system with a base pressure of 3×10^{-9} mbar by organic molecular beam epitaxy (O-MBE). The organic layers were evaporated from Knudssen cells, calibrating the growth rate with a quartz microbalance. A combined motorized sample holder-shutter system was used to grow a double wedge structure, controlling the speed of the shutter and the growth rate in order to produce a defined thickness gradient [7,12]. A 9-mm-long wedge of CuPc was grown with a rate of 0.03 Å/s and after a 90° rotation of the sample a second wedge of PTCBI was grown with the same rate (orthogonally to the first wedge). A uniform, 5-nm-thick layer of bathocuproine (BCP) was grown on top of the double wedge serving as hole blocking layer [13]. Finally, the fabrication was completed by depositing an 80-nm-thick silver cathode by means of an e-beam evaporator using a rate of 0.05 Å/s.

Recently, Raman spectroscopy has been demonstrated to be a valuable structural probe to complement photocurrent images in OPV devices [14]. In this work, Raman measurements were performed in ambient conditions using a WITec alpha300 RA+ setup with a 488 nm solid-state laser and a 633 nm He-Ne laser as excitation sources. The diffraction gratings had a density of 1200 and 600 grooves/mm, respectively. In all cases the objective employed had a 10× magnification and a 0.25 numerical aperture. The Raman images shown in this work contain ca. 20,000 spectra, which were acquired in lateral steps of 50 μm employing an integration time of 136 ms per spectrum. LBIC images consisted of more than 6000 data points and were acquired in a home-made setup using lateral steps of 100 μm. The LBIC experiments were performed non-modulated and with no bias. We have estimated the beam size after focusing with a 20× long working distance Mitutoyo objective to be ca. 20 μm (FWHM). The typical monochromatic power used was 44 μW for excitation with a 532 nm laser and 3,8 μW for the 630 nm monochromated light from a xenon lamp. Even though the 630 nm illumination was relatively low in our setup and thus normalization by incident power would lead to large errors in current density, we have still measured it as it corresponds to the maximum of the EQE in flat devices.

To assess the quality of the thickness gradients and for calibration purposes, single donor (acceptor) wedges were deposited on glass/ITO substrates using the same UHV techniques. The results of variable angle spectroscopic ellipsometry (VASE) and mechanical profilometry show a thickness profile which varies linearly as the light spot is displaced along the wedge (Fig. 1a). The inset in Fig. 1a confirms thicknesses ranging from ca. 20–200 nm in a 9 mm scanned length. Values obtained from single wedges were employed to extract the solid-state Raman cross-sections required to perform the quantification of film thickness in the functional device (Fig. 1c and d) [8]. The insets of Fig. 1c and d shows the Raman spectra of CuPc and PTCBI upon 488 nm excitation. For these materials, the most intense Raman bands do not overlap significantly, which facilitates their identification and ulterior thickness quantification. The optical constants of CuPc and PTCBI extracted from VASE are plotted in Fig. 1b and also used for the Raman cross section analysis (see below).

The characterization of the layers thicknesses by Raman spectroscopy is performed according to a previously reported quantitative model of the Raman intensity which was here adapted to the bilayer device geometry [8]. The methodology exploits the transfer-matrix formalism to describe the incoming and scattered electric fields in an optical system formed by an arbitrary number of layers. This allows modelling the scattered Raman intensity as a function of the Raman-active layer thickness as well as the volumetric composition in the case of multi-component blends. Here, we have reformulated the mathematical approach of the methodology initially presented in Ref. [8] to include two film thickness values, d_1 and d_2, as free parameters for the fit of the experimental Raman spectra instead of the single thickness value, d, and a volumetric fraction, v, as occurs for an homogeneous blend. The model takes into consideration the fact that the scattered intensity of each Raman-active layer depends simultaneously on its own thickness and on the thickness of the other Raman-active layer to properly account for the filtering effect that each layer has on the incoming and scattered fields. Thus, the model function of the scattered intensity (I) reads

$$I(d_1, d_2) = \sigma_1 f_1(d_1, d_2) I_{ref,1} + \sigma_2 f_2(d_1, d_2) I_{ref,2} \quad (1)$$

where $\sigma_{1,2}$ are the effective Raman cross-sections of materials 1 and 2 in solid-state, $f_{1,2}$ describe the Raman intensity vs. film thickness dependence obtained by means of the transfer-matrix formalism for the layers containing materials 1 and 2, and $I_{ref,1,2}$ are the reference Raman spectra of materials 1 and 2 at the excitation wavelength and normalized to the Raman band to which $\sigma_{1,2}$ are referred. The n and k values of each layer are used as input parameters in the modelling (Fig. 1b). Further details on the mathematical formulation of the model and the Raman cross-sections can be found in Ref. [8]. For the present case and experimental conditions (488 nm excitation), the Raman cross-section ratio between PTCBI and CuPc was found to be PTCBI/CuPc = 18 ± 2 for their most intense vibrational bands at 1290 and 1528 cm^{-1}, respectively. The moderate value of the ratio is beneficial for the Raman characterization as it allows a good sensitivity during the fit [8].

We then used the model and calibrated cross sections to analyze the Raman signal obtained through the glass substrate of a complete device. The fits of the Raman spectra according to Eq. (1) are generally very good, as shown in Fig. 2 for three representative examples. These fits lead to film thickness maps in which both CuPc and PTCBI wedges can be visualized and quantified as illustrated in Fig. 2. According to this analysis, both wedges are not strictly orthogonal (Fig. 2a and b) but lead to a rather homogeneous total thickness of 15–20 nm (Fig. 2c). The reason for the imperfect orthogonality of the wedges is the divergence of the evaporation cone, which gives raise to thickness inhomogeneity along the axis perpendicular to the gradient. This fact can be minimized by collimating the evaporation cone (using deep crucibles with lower aperture) and reducing the distances between the evaporation source and the substrate but it is difficult to avoid completely in our current O-MBE setup.

LBIC-based photocurrent images are illustrated in Fig. 3 at two different excitation wavelengths, namely 532 nm and 630 nm. According to the absorption spectra of CuPc and PTCBI illustrated in Fig. 1b, PTCBI is the major absorber of the bilayer at 532 nm excitation, thus the variation of the photocurrent measured at such wavelength would correspond to the increased absorption of light due to the larger PTCBI thickness. This is confirmed by the general agreement between Figs. 2b and 3b, showing both images a monotonically decreasing trend in Raman intensity and 532 nm photogenerated current density, respectively, from left to right following the slope of the PTCBI wedge. Note that as the electrode of the device is continuous, the low photocurrent blue spots that appear on the left hand side in Fig. 3b do not correspond to dead pixels as such, but rather to large fluctuations in the

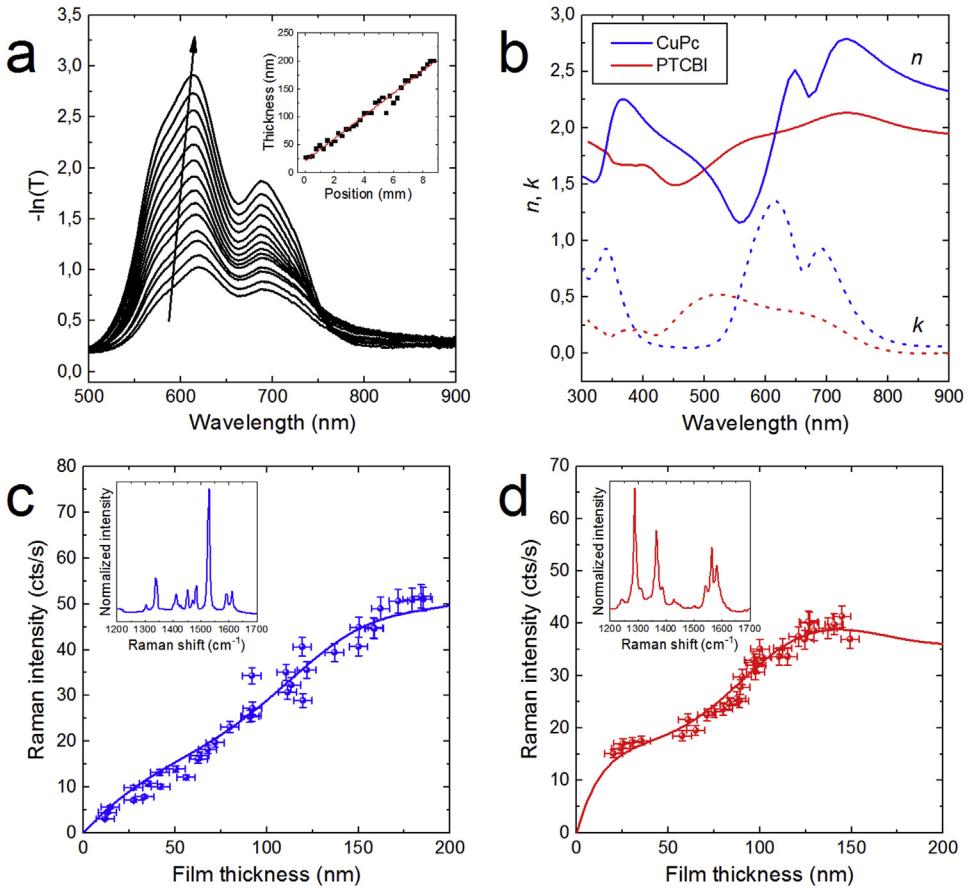

Fig. 1. (a) Single CuPc wedge layer absorbance as a function of position and (inset) thicknesses obtained by profilometry fitted to a linear equation as a guide to the eye. The arrow displayed in the absorbance spectra indicates their evolution as the thickness increases. (b) Refractive index (n, solid lines) and extinction coefficient (k, dashed lines) of CuPc (blue) and PTCBI (red) measured with VASE. (c) Intensity of the 1528 cm^{-1} mode of CuPc as a function of film thickness. The solid line stands for the fit of the model introduced in Ref. [8]. The inset shows the normalized Raman spectrum of CuPc at 488 nm excitation. (d) Intensity of the 1290 cm^{-1} mode of PTCBI as a function of film thickness and fit of the experimental data according to the transfer-matrix model in Ref. [8]. The inset shows the normalized Raman spectrum of PTCBI at 488 nm excitation. (For interpretation of the references to color in this figure legend, the reader is referred to the Web version of this article.)

photocurrent readings that have to do with the fast acquisition times for the Keithley source-meter and the home-made LabView interface developed to control the LBIC setup. We have repeatedly tested that such photocurrent spikes are not related to the sample or the excitation wavelength.

At 630 nm excitation both materials are absorbing and the

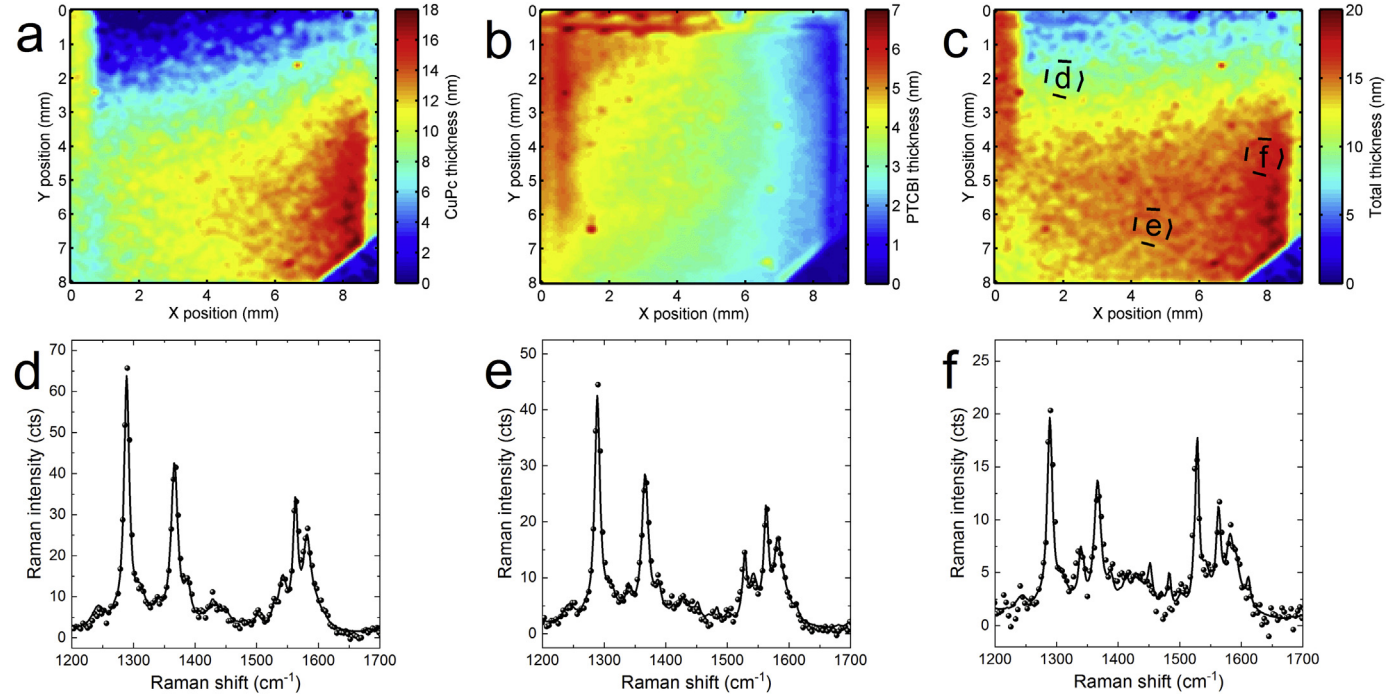

Fig. 2. Thickness spatial maps corresponding to (a) CuPc thickness, (b) PTCBI thickness and (c) total active layer thickness as extracted from Raman spectroscopy upon 488 nm excitation. (d), (e) and (f) show the experimental Raman spectra (circles) as well as the fits performed according to Eq. (1) (solid lines) at the sample locations indicated in (c).

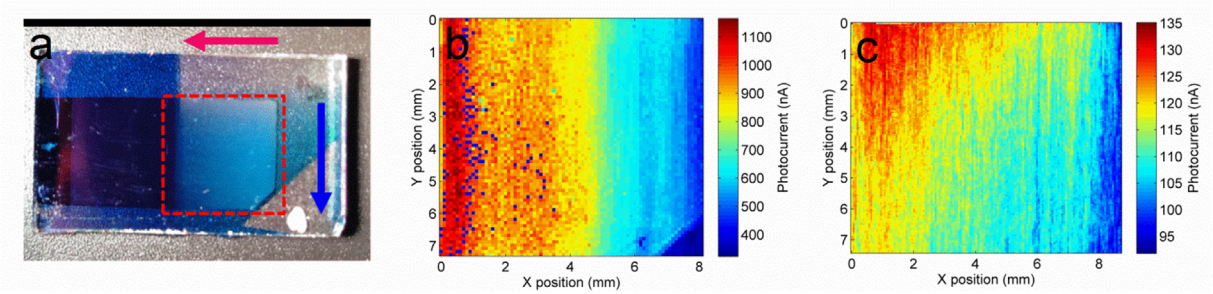

Fig. 3. (a) Photograph of the device active area. The pink and the blue arrows show the PTCBI and the CuPc gradient directions, respectively. (b) LBIC image at 532 nm excitation wavelength. (c) LBIC image at 630 nm excitation wavelength. LBIC images were taken on the area marked with a dashed line in (a). (For interpretation of the references to color in this figure legend, the reader is referred to the Web version of this article.)

photocurrent image shows a diagonal trend indicating the area where the balance between exciton diffusion and light absorption is optimized. Interestingly, the variation of CuPc thickness observed in Fig. 2a follows the same trend observed on the LBIC map at 630 nm (Fig. 3c) indicating that a small amount of CuPc is enough for good device performance. Note that while the overall photocurrent of the device cannot be extracted from a single wavelength measurement, the photocurrent contribution is expected to be the highest at 630 nm as is the case for incident photon-to-current efficiency (IPCE) measurements on flat bilayer devices.

The spatial correlation of the Raman-based thickness maps with the photocurrent images measured in the LBIC setup enables the fast combinatorial evaluation of the bilayer system. Nevertheless, since both datasets are acquired in different setups the comparison requires the proper matching of both maps by rotation and interpolation. First, using defects in the sample and sample edges, the images are slightly rotated to accommodate differences in positioning between setups. Then the pixel correlation is performed by interpolation of the map with the highest resolution. The regions showing the highest photocurrent generally correspond to those in which the light absorption, the exciton diffusion and the charge collection are optimized to yield a high IPCE in the system studied. In the here analyzed bilayer model system, the correlation between the active layer thicknesses and the photocurrent measured at 532 and 630 nm (Fig. 4a and b) indicates that a single photocurrent maximum occurs at ca. 10 nm of CuPc and ca. 5 nm of PTCBI. This thickness difference might be related to the lower extinction coefficient of PTCBI with respect to CuPc (Fig. 1b) or to difference in exciton diffusion lengths. The colored dispersion of photocurrent in Fig. 4a and b is in good agreement with previously reported works performed on devices with a similar architecture [2,4,13]. We do not observe oscillations in the photocurrent as a function of the active layer thickness as reported elsewhere and ascribed to optical interference effects [3] since we are in the very thin film thickness regime.

Typical optimization approaches in which the thickness of each active layer is varied in discrete steps while keeping the other film thicknesses constant require fabricating a minimum of 10–20 individual samples to find the optimum solution to the multi-parametric problem [3,4,15]. In order to better visualize the advantages of our gradient-based combinatorial approach, we quantify the time saving (S) parameter according to the following expression:

$$S = \frac{N_{dev}(t_{fab} + t_{JV})}{t_{fab} + N_{pts} t_{LBIC}} \quad (2)$$

where N_{dev} is the number of discrete devices fabricated; t_{fab} is the average time required to fabricate each device which equals the time required to fabricate a single double-wedged device; t_{JV} is the time required to measure the J-V curve in a single flat device; N_{pts} is the number of photocurrent data points extracted at the LBIC setup; and t_{LBIC} is the measurement time required per LBIC data point. The optimization of the fabrication recipe can reduce t_{fab} up to ca. 3 h, whereas t_{JV} is typically not longer than 3 min per sample and t_{LBIC} equals ca. 1 s per data point. When $N_{dev} = N_{pts}$ and using the above-cited values for t_{fab}, t_{JV} and t_{LBIC}, Eq. (2) leads to $S \approx N_{dev}$, thus for a typical optimization routine using discrete samples in which the number of fabricated devices raises up to 20 units ($N_{dev} = N_{pts} = 20$), the combinatorial approach is ca. 20 times faster than the discrete approximation and also ca. 20 times more efficient in terms of use of resources and energy. Keeping $N_{dev} = 20$ but increasing N_{pts} up to 2000 results in $S \approx 17$ while having a hundred-fold increase in the number of data points available to solve the multi-parametric problem with respect to a discrete approach. Importantly, the savings in the amount of material required for the optimization is of the order of N_{dev}. Clearly, the combinatorial method presented here is significantly more efficient on the fabrication and measuring time employed for multi-parametric optimization problems.

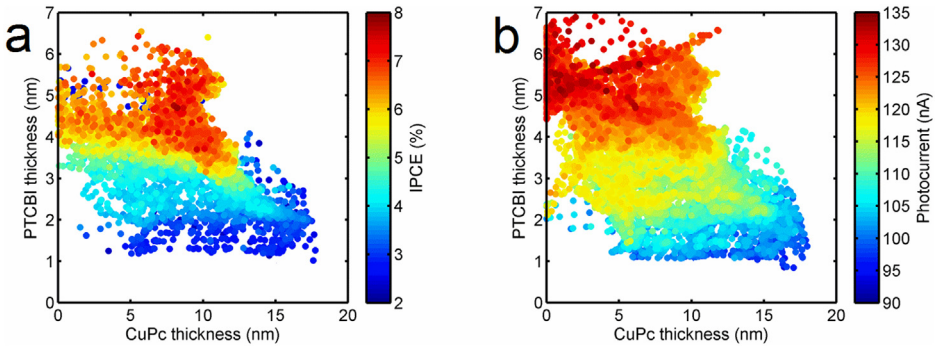

Fig. 4. (a) Incident photon-to-current conversion efficiency IPCE (%) at 532 nm excitation wavelength and (b) short circuit photocurrent at 630 nm excitation wavelength.

3. Conclusion

In summary, we have developed a combinatorial approach for the optimization of the performance of small molecule organic solar cells which implies a ca. 20-fold reduction in the consumption of resources and time with respect to a discrete optimization routine. The optimization is performed using a single functional device showing orthogonally oriented, wedged donor-acceptor layers to study the influence of their thickness on the final photoconversion efficiency. The successive local characterization with LBIC and quantitative Raman spectroscopy enables the correlation of the IPCE with the thickness of the active layers. In the case of CuPc and PTCBI heterojunction solar cells, the optimum device performance results from a trade-off between exciton diffusion and light absorption. For the device architecture studied in this work we found that the photocurrent achieved its maximum for CuPc and PTCBI layer thicknesses equal to ca. 10 nm and 5 nm, respectively. The here presented combinatorial screening methodology can be applied in any evaporated thin-film-based solar cell technology, potentially including tandem geometry and other complex multilayered architectures such OLEDs.

Acknowledgements

The Spanish Ministerio de Economía y Competitividad (MINECO) is gratefully acknowledged for its support through Grant No. SEV-2015-0496 in the framework of the Spanish Severo Ochoa Centre of Excellence program. J.C.-G. acknowledges funding from the MINECO through projects MAT2014-57652-C2-1-R and PCIN-2015-169-C02-01 and from the Madrid Regional Government through MAD2D project. M.A.N. acknowledges support from the MINECO through MAT2014-59315-R project. G.L. thanks the China Scholarship Council for financial support (201406790019). X.R.-M., A.S.-D. and M.C.-Q. acknowledge financial support from the European Research Council through project ERC CoG648901.

References

[1] C.W. Tang, Two-layer organic photovoltaic cell, Appl. Phys. Lett. 48 (1986) 183–185, http://dx.doi.org/10.1063/1.96937.
[2] V.P. Singh, R.S. Singh, B. Parthasarathy, A. Aguilera, J. Anthony, M. Payne, Copper-phthalocyanine-based organic solar cells with high open-circuit voltage, Appl. Phys. Lett. 86 (2005) 82106, http://dx.doi.org/10.1063/1.1871347.
[3] T. Stübinger, W. Brütting, Exciton diffusion and optical interference in organic donor–acceptor photovoltaic cells, J. Appl. Phys. 90 (2001) 3632–3641, http://dx.doi.org/10.1063/1.1394920.
[4] X. Tong, R.F. Bailey-Salzman, G. Wei, S.R. Forrest, Inverted small molecule organic photovoltaic cells on reflective substrates, Appl. Phys. Lett. 93 (2008) 173304, http://dx.doi.org/10.1063/1.3005173.
[5] S.W. Hur, H.S. Oh, Y.C. Oh, D.H. Chung, J.U. Lee, J.W. Park, T.W. Kim, Organic photovoltaic effects using CuPc and C60 depending on layer thickness, Synth. Met. 154 (2005) 49–52, http://dx.doi.org/10.1016/j.synthmet.2005.07.020.
[6] J. Cabanillas-Gonzalez, M. Schmidt, O. Peña-Rodríguez, M.I. Alonso, A.R. Goñi, M. Campoy-Quiles, Effect of structure and interlayer diffusion in organic position sensitive photodetectors based on complementary wedge donor/acceptor layers, J. Nanosci. Nanotechnol. 13 (2013) 5148–5153, http://dx.doi.org/10.1166/jnn.2013.7503.
[7] M. Campoy-Quiles, V. Randon, M.M. Mróz, M. Jarzaguet, M. Garriga, J. Cabanillas-González, Continuous lateral gradients in film morphology for position sensitive detection and organic solar cell optimization, Org. Photonics Photovoltaics 1 (2013), http://dx.doi.org/10.2478/oph-2013-0002.
[8] X. Rodríguez-Martínez, M.S. Vezie, X. Shi, I. McCulloch, J. Nelson, A.R. Goñi, M. Campoy-Quiles, Quantifying local thickness and composition in thin films of organic photovoltaic blends by Raman scattering, J. Mater. Chem. C 5 (2017) 7270–7282, http://dx.doi.org/10.1039/C7TC01472D.
[9] S. Klinkhammer, X. Liu, K. Huska, Y. Shen, S. Vanderheiden, S. Valouch, C. Vannahme, S. Bräse, T. Mappes, U. Lemmer, Continuously tunable solution-processed organic semiconductor DFB lasers pumped by laser diode, Optic Express 20 (2012) 6357, http://dx.doi.org/10.1364/OE.20.006357.
[10] S. Höfle, T. Lutz, A. Egel, F. Nickel, S.W. Kettlitz, G. Gomard, U. Lemmer, A. Colsmann, Influence of the emission layer thickness on the optoelectronic properties of solution processed organic light-emitting diodes, ACS Photonics 1 (2014) 968–973, http://dx.doi.org/10.1021/ph500186m.
[11] F. Nickel, C. Sprau, M.F.G. Klein, P. Kapetana, N. Christ, X. Liu, S. Klinkhammer, U. Lemmer, A. Colsmann, Spatial mapping of photocurrents in organic solar cells comprising wedge-shaped absorber layers for an efficient material screening, Sol. Energy Mater. Sol. Cells 104 (2012) 18–22, http://dx.doi.org/10.1016/j.solmat.2012.04.026.
[12] J. Cabanillas–Gonzalez, O. Peña–Rodríguez, I. Suarez Lopez, M. Schmidt, M.I. Alonso, A.R. Goñi, M. Campoy–Quiles, Organic position sensitive photodetectors based on lateral donor-acceptor concentration gradients, Appl. Phys. Lett. 99 (2011) 103305, http://dx.doi.org/10.1063/1.3631731.
[13] P. Peumans, V. Bulović, S.R. Forrest, Efficient photon harvesting at high optical intensities in ultrathin organic double-heterostructure photovoltaic diodes, Appl. Phys. Lett. 76 (2000) 2650–2652, http://dx.doi.org/10.1063/1.126433.
[14] J. Gao, A.K. Thomas, J. Yang, C. Aldaz, G. Yang, Y. Qin, J.K. Grey, Polythienylene–vinylene structure–function correlations revealed from resonance Raman spectroscopy and photocurrent imaging, J. Phys. Chem. C 119 (2015) 8980–8990, http://dx.doi.org/10.1021/acs.jpcc.5b02166.
[15] D.W. Sievers, V. Shrotriya, Y. Yang, Modeling optical effects and thickness dependent current in polymer bulk-heterojunction solar cells, J. Appl. Phys. 100 (2006) 114509, http://dx.doi.org/10.1063/1.2388854.